Cement and Concrete Research 138 (2020) 106248

Contents lists available at ScienceDirect

Cement and Concrete Research

journal homepage: www.elsevier.com/locate/cemconres

Effect of sulfate on C-S-H at early age

Elise M.J. Bérodier, Arnaud C.A. Muller*, Karen L. Scrivener

Laboratory of Construction Materials (LMC), Swiss Federal Institute of Technology (EPFL), Station 12, CH-1015 Lausanne, Switzerland

ARTICLE INFO

Keywords:
Cement
Sulfate
C-S-H
Morphology
Gel water
Pores
NMR
SEM
XRD
Calorimetry

ABSTRACT

The effect of increasing sulfate contents on the hydration of white cement was studied with a multi-technique approach. Quantitative X-Ray Diffraction (XRD) revealed that adding more gypsum in the cement resulted in more ettringite formation. Combining isothermal calorimetry, advanced in-situ ^{1}H nuclear magnetic resonance (NMR) and early scanning electron microscopy (SEM) observations, it was possible to correlate the depletion of the gypsum with a change in C-S-H morphology, from needle-like to agglomerated C-S-H, together with a change in C-S-H gel pore content. Nevertheless, the content of C-S-H interlayer water remained similar and no change in C-S-H pore sizes were observed when increasing the sulfate content. The data allowed to calculate the volume composition of hydrated cement pastes at 3 days of hydration. The more gypsum was added to the cement, the lower was the bulk C-S-H volume due to lower gel pore content and the higher was the content of capillary porosity.

1. Introduction

Gypsum is a critical component of Portland cements. About 4–5% of gypsum is usually added to the clinker during grinding. The first function of the gypsum is to control the reaction of the C_3A phase and to avoid flash set. On the other hand, too much gypsum has been seen to cause expansion due to ettringite formation. In the cement and concrete industry, the optimum gypsum is typically chosen empirically by checking both setting time and strength development. Isothermal calorimetry can alternatively be used to adjust the gypsum content from the intensity and position of the aluminate peak (ideally located between 10 and 24 h of hydration). Despite the primary function of calcium sulfate as a set regulator, its impact on the phase assemblage, on the C-S-H at early age (< 2 days), and on the strength development is more complicated to understand and less documented.

Calcium sulfate has been known since more than 100 years to regulate the C_3A reaction [1]. The slow-down of the C_3A reaction in presence of sulfate phases was often attributed to the formation of a layer of ettringite around the clinker particles, hindering further C_3A dissolution [2–4], but the ettringite crystals formed are quite discreet and would not present a barrier to chemical reaction. Initially suggested by Feldman and Ramachandran [5] in 1966, the theory of inhibition of C_3A dissolution by the presence of sulfate ions in solution, which absorb on reactive surface sites and slow down dissolution, is getting more support from recent works [6,7]. The presence of calcium sulfate in Portland cements leads first to ettringite formation. After that the calcium sulfate phases have been consumed (gypsum, bassanite or anhydrite), a renewal of the C_3A reaction is observed. In Portland cement systems, where sulfate is initially absorbed on C-S-H, this leads first to more ettringite formation, taking sulfate out of C-S-H, and then to the formation of AFm phases: monosulfoaluminate or mono/hemi carboaluminate.

Zeta potential measurements have shown that sulfate is easily adsorbed on/in calcium silicate hydrates (C-S-H) [8]. The amount of sulfate absorbed by the C-S-H during hydration is high enough to be detected by energy-dispersive X-ray spectroscopy with typical values of S/Ca of 0.1. A positive correlation between the Ca/Si ratio and the sulfate content of the C-S-H was found [9]. It is believed that the sulfate ions are adsorbed as $CaSO_3$ complexes and not incorporated in the atomic structure of the C-S-H. A study from Labbez et al. [10] and a model from Barbarulo et al. [11] well supported this theory and indicated that $CaSO_3$ complexes are adsorbed on SiO sites. This surface interaction seems to be reversible and sulfate ions can be released from C-S-H when the sulfate content in the pore solution drops. Therefore the formation of sulfoaluminate phases can continue while the gypsum from the cement is depleted [12].

The impact of sulfates on the C-S-H morphology is rarely reported. Several authors have suggested that calcium sulfate might change the growth of C-S-H in cement paste owing to the possible adsorption of the sulfate species on the C-S-H structure [11,13]. A recent work showed a more convergent structure of C-S-H needles in alite pastes containing sulfate [14].

* Corresponding author at: HeidelbergCement AG, Oberklamweg 2-4, 69181 Leimen, Germany.
E-mail address: arnaud.muller@heidelbergcement.com (A.C.A. Muller).

https://doi.org/10.1016/j.cemconres.2020.106248
Received 20 May 2020; Received in revised form 29 September 2020; Accepted 30 September 2020
Available online 15 October 2020

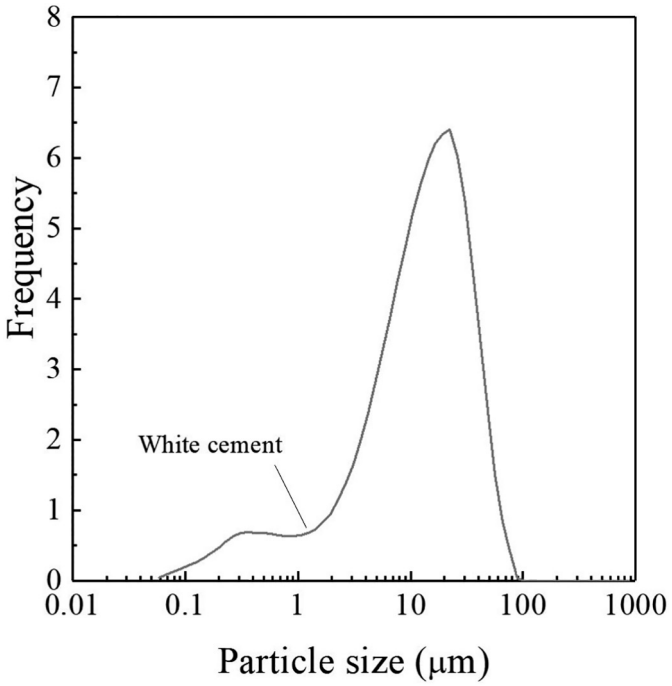

Fig. 1. Particle size distribution of the white cement used in this study.

In this paper, the effect of different sulfate contents on the hydration of white cement was studied with a multi-technique approach including isothermal calorimetry, quantitative X-Ray Diffraction (XRD), advanced in-situ ^{1}H nuclear magnetic resonance (NMR) and early scanning electron microscopy (SEM) observations.

2. Materials and methods

2.1. Materials and casting procedure

White Portland cement was used in this study. It contained approximately 67% C_3S, 20% C_2S, 3.6% C_3A, 2.6% anhydrite, 2.1% bassanite with all other phases less than 1% of the total (by XRD Rietveld quantification). The SO_3 content determined by XRF analysis was 2.1%. The particle size distribution of the white cement is shown in Fig. 1.

Typically 80 g of anhydrous white cement was mixed with water at a water-to-cement, $w/c = 0.40$, for 2 min at 1600 rpm with a paste mixer LABORTECHNIK RW 20.n. When required, additional 2% and 4% gypsum by weight (not already in the cement) were blended together with the cement in a turbula blender for 10 min. The gypsum used was a commercially available high purity gypsum powder. This led to 2.94% and 3.87% total SO_3 with respect to the mass of cement, for 2% and 4% of extra gypsum, respectively. Following the same procedure as for the plain white cement, 80 g of these dry mixtures were then mixed with water. All fresh pastes were directly placed into sealed plastic containers (for XRD and microscopy measurements) and into sealed NMR tubes (for ^{1}H NMR measurements). In addition, in-situ XRD and isothermal calorimetry measurements were carried out. All samples were kept at 20 °C and sealed throughout the hydration.

2.2. Measurement methods

Each cement was tested for compressive strength according to the European standard EN 196 at 3, 7 and 28 days of hydration.

The overall kinetics of hydration were recorded with an isothermal calorimeter (TAM Air from TA Instruments). It consists of 8 parallel twin measurement channels maintained at a constant temperature: one for the paste sample (approximately 10 g), the other for the reference sample. The instrument was maintained in a temperature controlled room to ensure the stability of the baseline. Measurements were carried out for 3 days at 20 °C.

In-situ X-Ray Diffraction (XRD) was used to follow the phase assemblage at early age. The pastes were prepared externally and then placed in a temperature controlled XRD sample holder. Measurements were carried out at 20 °C for 40 h. The acquisition time for one diffraction pattern was 15 min. A Panalatical X'Pert Pro MPD diffractometer in a θ-θ configuration was used with a CuKα source (wavelength 1.54 Å) and a fixed divergence slit of 0.5°. Samples were scanned on a rotating stage between 7 and 70° (2θ) using a X'Celerator detector with a step size of 0.0167° (2θ) and a time step of 77.5 s. Other samples cured for longer times were analysed by XRD after immersion in isopropanol for 7 days and after drying under vacuum in a desiccator for 7 days over silica gel. Rietveld analysis was done on all samples with the external standard method. The standard used in this work was rutile powder supplied by Kronos (2300 Titanium dioxide).

The cement microstructure was observed on polished sections with scanning electron microscopy (SEM). Pieces of dried sample were impregnated using epoxy-based EPO-TEK® 301 resin and polished at 150 rpm with a STRUERS Rotopol machine using different size diamond sprays and petrol as a lubricant. The sample was then coated with a 30 nm carbon film using a BAL-TEC CED 030 Carbon Evaporator. The SEM used to observe the polished sections was a FEI Quanta 200 equipped with a tungsten filament. The spot size was adjusted to yield a 0.7–0.8 nA current. Observations in the SEM were done in high vacuum conditions (5×10^{-5} Pa) using backscattered electron imaging (BSE) at 15 kV.

The C-S-H morphology was observed with a FEI XLF-30 SFEG-SEM for secondary electron images. The hydration occurring in the cement paste was stopped before analysis by solvent exchange with isopropanol, a process known as the most adequate and gentle procedure for microstructural observation. At the required times, 0.2 g of paste was taken out from the sealed samples and put in a filtrating funnel with two filter papers (retention 5 μm). The funnel was immediately filled with isopropanol and the sample stirred in the funnel for 2 min. Then the isopropanol was removed with a vacuum pump. The procedure was repeated four times. Once the isopropanol was removed, the dried paste was collected from the filter paper and stored under vacuum in a desiccator for 5 days over silica gel.

^{1}H proton Nuclear magnetic resonance (NMR) measurements were carried out on a Bruker Minispec NMR spectrometer operating at 7.5 MHz. CPMG and Quad-Echo measurements were carried out alternatively to monitor the kinetic of the water in-situ throughout the hydration. Measurement parameters and analysis were identical to the ones reported in [15–17]. In this configuration all the water inside hydrating cement pastes can be detected and quantified. The differentiation between the different water populations is discussed along with the results in Section 3.5.

3. Results

3.1. Compressive strengths

The three white cement systems were tested for compressive strength according to the European standard EN 196 at 3, 7 and 28 days of hydration. The results are presented in Fig. 2 as a function of the SO_3 level of the cement. The addition of 2% gypsum to the white cement increased the compressive strength of mortars at all tested ages. However, going to 4% extra gypsum led to a reduction of strength. The decrease of strength between 2% and 4% extra gypsum was more pronounced at 3 days compared to 7 or 28 days, times at which further hydration has taken place. The intermediate sulfate content (mix with 2.94% SO_3) appears to be close to the optimum with respect to compressive strength development.

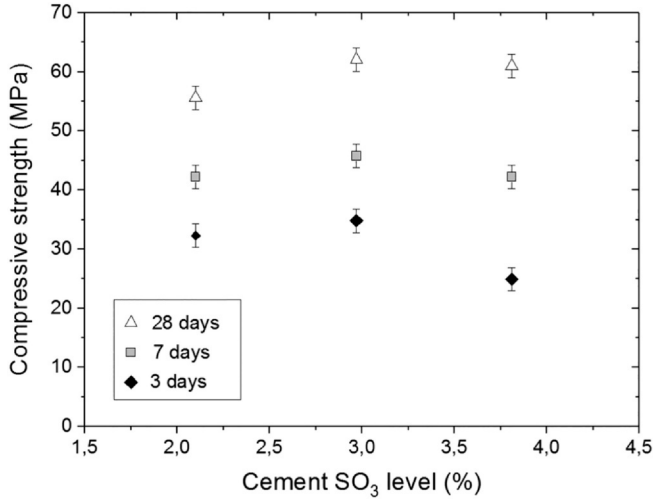

Fig. 2. Compressive strength of standardized mortars for the plain white cement and the cements with 2% and 4% extra gypsum at 3, 7 and 28 days of hydration. The data are presented as a function of the total sulfate content in the dry mix.

3.2. Isothermal calorimetry

Fig. 3 shows the calorimetry results for the plain white cement paste and the pastes prepared with 2% and 4% additional gypsum over the first 3 days of hydration. The calorimetry curve for Portland cements is typically composed of 4 stages: a fast initial dissolution, an "induction" period, an acceleration and a deceleration period. The results presented in Fig. 3 show that the first 3 stages of hydration are not significantly affected by the presence of additional sulfate as the 3 curves overlap up to the main peak. In particular the acceleration period of the alite reaction is not affected by a change of sulfate content. The kinetics of the aluminate reaction (C_3A), occurring during the deceleration period and characterized by the second calorimetry peak, is however significantly modified by a change in sulfate content. The plain white cement paste has a strong and sharp aluminate peak at around 12 h of hydration. Between 30 and 45 h, a smaller, broader secondary aluminate peak is observed. When 2% of extra gypsum was added to the cement (2.94% total SO_3), the primary aluminate peak is delayed from 12 h to 16 h and significantly reduced in height. There is no secondary aluminate peak

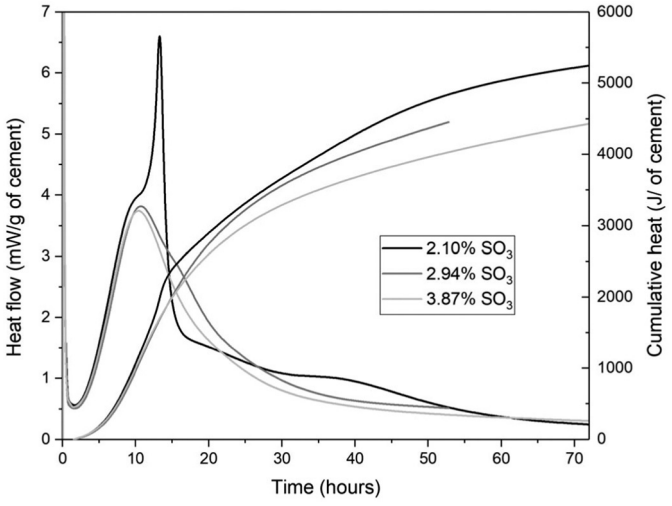

Fig. 3. Isothermal calorimetry results of the plain white cement paste and the white cement pastes prepared with 2% and 4% of extra gypsum. Gypsum addition mainly affects the peak related to the aluminate reaction. The system with 2% extra gypsum was measured only until 53 h.

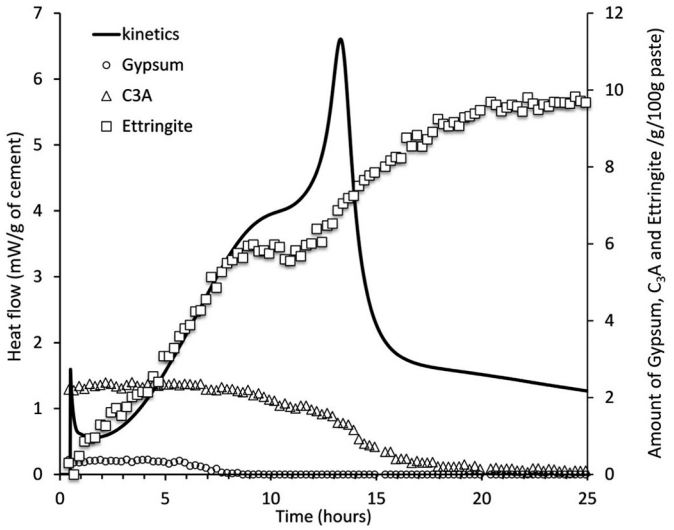

Fig. 4. In-situ XRD measurements of the plain white cement paste showing the consumption of C_3A and gypsum and the formation of ettringite (by Rietveld analysis) as a function of hydration time.

observed within the first 72 h. When 4% of extra gypsum was added to the cement (3.87% total SO_3), the calorimetry results do not show any aluminate peak within the first 72 h of hydration.

Cumulative heat results at 2–3 days show that mixes with additional gypsum generate less heat than the plain white cement paste due to the delay of the aluminate reaction.

3.3. XRD measurements

Measuring XRD on in situ sample allows showing the phase assemblage evolution. Fig. 4 focus on the consumption of C_3A and gypsum and on the formation of ettringite for the plain white cement paste over the first 24 h of hydration, as measured by in-situ XRD. The results confirm that the sharp peak seen at 12 h on the calorimetry results (Fig. 3) corresponds to a surge of C_3A dissolution and the parallel formation of ettringite. The content of ettringite goes from 5.8 g/100 g of paste at 11 h to 9.7 g/100 g of paste at 24 h (equivalent to 13.6 g/100 g of anhydrous cement). The formation of ettringite from the sudden C_3A reaction is observed even though gypsum is not anymore detected by XRD (gypsum depletion has happened at around 8 h). The formation of ettringite in the absence of calcium sulfate phases was already observed by Quennoz et al. [12] and Gallucci et al. [18] and was attribute to the aluminate reaction with the remaining sulfate in solution and with the sulfate desorbing from the C-S-H. The formation of ettringite in the present study reaches a plateau at around 22 h likely due to the complete depletion of C_3A.

The degree of hydration of the cement and of each of the three main clinker phases alite, belite and aluminate was measured by QXRD at 3 days of hydration. The results are shown in Fig. 5 for the three pastes studied. At 3 days, the degree of hydration of the aluminate is decreased with the presence of extra sulfate in the cement. The same can also be observed for alite, but to a lower extent. On the contrary, belite tends to react more in the presence of extra sulfate. At 3 days, the plain white cement and the cements with 2% and 4% extra gypsum have degrees of hydration (including the extra gypsum) of 0.63, 0.61 and 0.59, respectively.

The amount of Portlandite and ettringite quantified by XRD at 3 days of hydration is shown in Fig. 6 as a function of the total SO_3 content of the cement. As expected, the addition of extra sulfate led to more ettringite formation. The plain white cement paste has 9.9 g of ettringite/100 g of anhydrous cement at 3 days of hydration. In comparison, the paste with 2% extra gypsum contains 12.3 g of ettringite

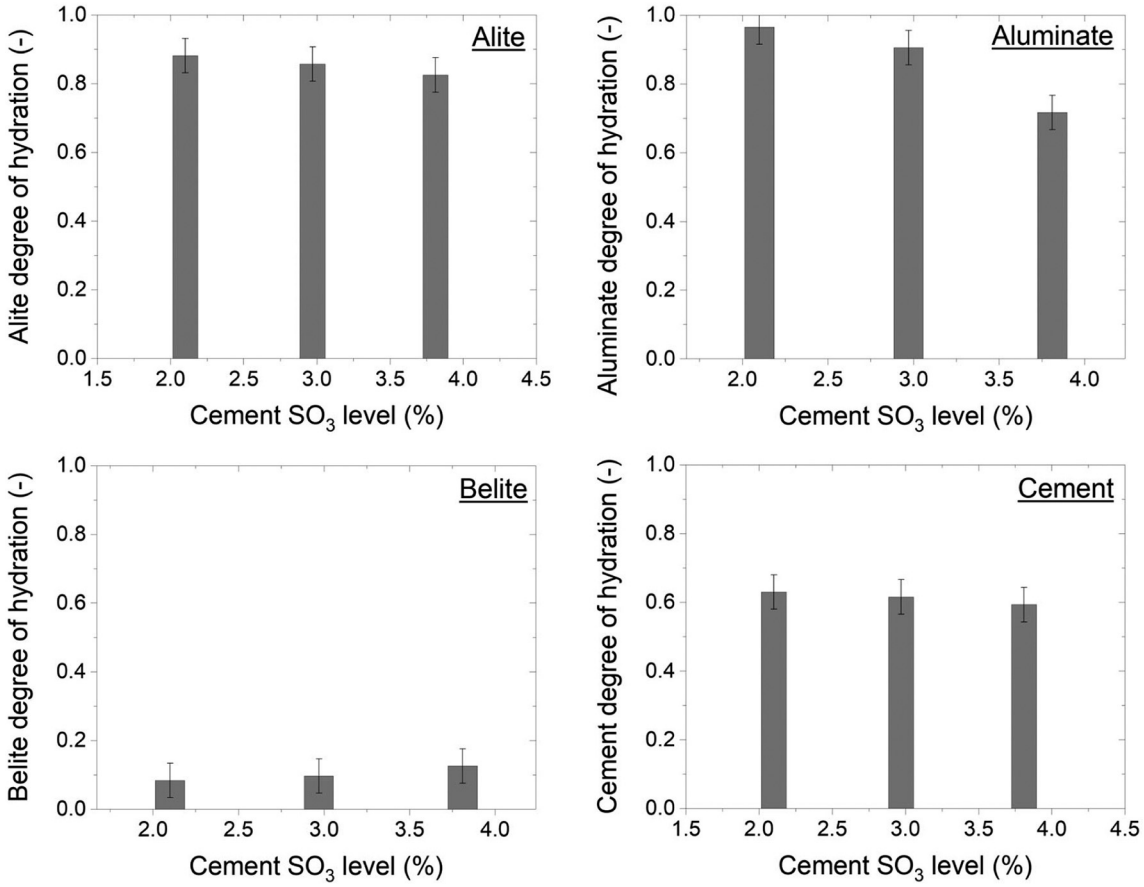

Fig. 5. Degree of hydration at 3 days of the main clinker phases and of the cement (including gypsum) as a function of the total sulfate content of the cement. The error of the quantitative XRD method is ± 5%.

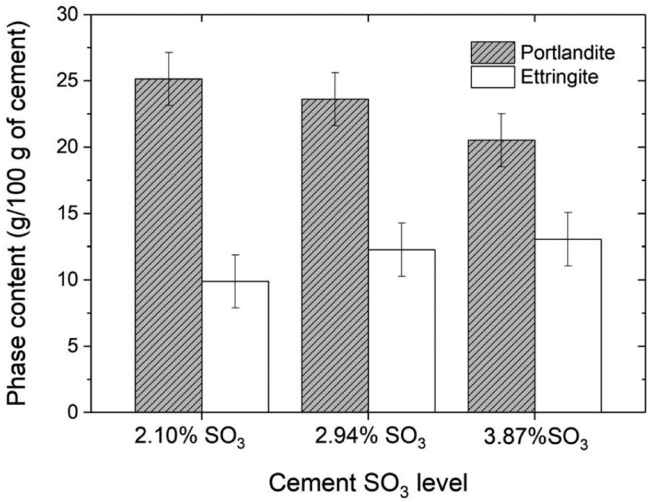

Fig. 6. Mass of Portlandite and ettringite, in g/100 g of anhydrous cement, measured and quantified by XRD at 3 days of hydration. The data are presented as a function of the total SO_3 content of the cement.

and the paste with 4% extra gypsum has 13.1 g of ettringite/100 g of cement. The ettringite content for the plain white cement paste presented in Fig. 6 is slightly lower than the in-situ XRD results presented in Fig. 4 (9.7 g/100 g of paste or 13.6 g/100 g of cement). This may be the result of the partial decomposition of ettringite upon hydration stoppage and sample preparation for the ex-situ QXRD.

The Portlandite content shows the opposite trend of the ettringite content: the more sulfate is added to the cement the less Portlandite is formed. This is partially explained by the lower degree of alite hydration shown in Fig. 5.

3.4. SFEG-SEM microscopy

The morphology of cement hydrates was observed by SFEG-SEM microscopy over the course of the deceleration period for each mix.

Fig. 7 a,b,c show the C-S-H morphology development before, during and after the C_3A peak as identified on the calorimetry curve for the plain white cement paste. At 10 h, the C-S-H appears as diverging needles growing outward from the cement particles. At 13 h of hydration which corresponds to the maximum of the C_3A peak, the C-S-H needle morphology is less defined and a new type of C-S-H is formed with a more “agglomerated” type of morphology. By 16 h, after the C_3A peak, the newly formed C-S-H appears even more agglomerated. These SEM observations, combined with calorimetry and in-situ XRD results (Fig. 3 and Fig. 4), suggest that there is a morphology transition from divergent needles to “agglomerated C-S-H” and that this phenomenon correlates with the depletion of the gypsum.

Fig. 7 d,e,f show the C-S-H morphology at 13, 16 and 20 h of hydration for the white cement paste prepared with 2% extra gypsum. Using the same method, these times correspond to the times before, during and after the C_3A peak. A similar transition of the C-S-H morphology as for the plain white cement paste is observed. Before the aluminate peak, the C-S-H have the divergent needle morphology. At the aluminate peak (16 h), the needles are less defined. At 20 h, the C-S-H are more agglomerated on each other. Again, the transition from divergent needles to agglomerated morphology correlates with the respective time of gypsum depletion.

Fig. 7 g,h,i show the C-S-H morphology at 13, 16 and 20 h of

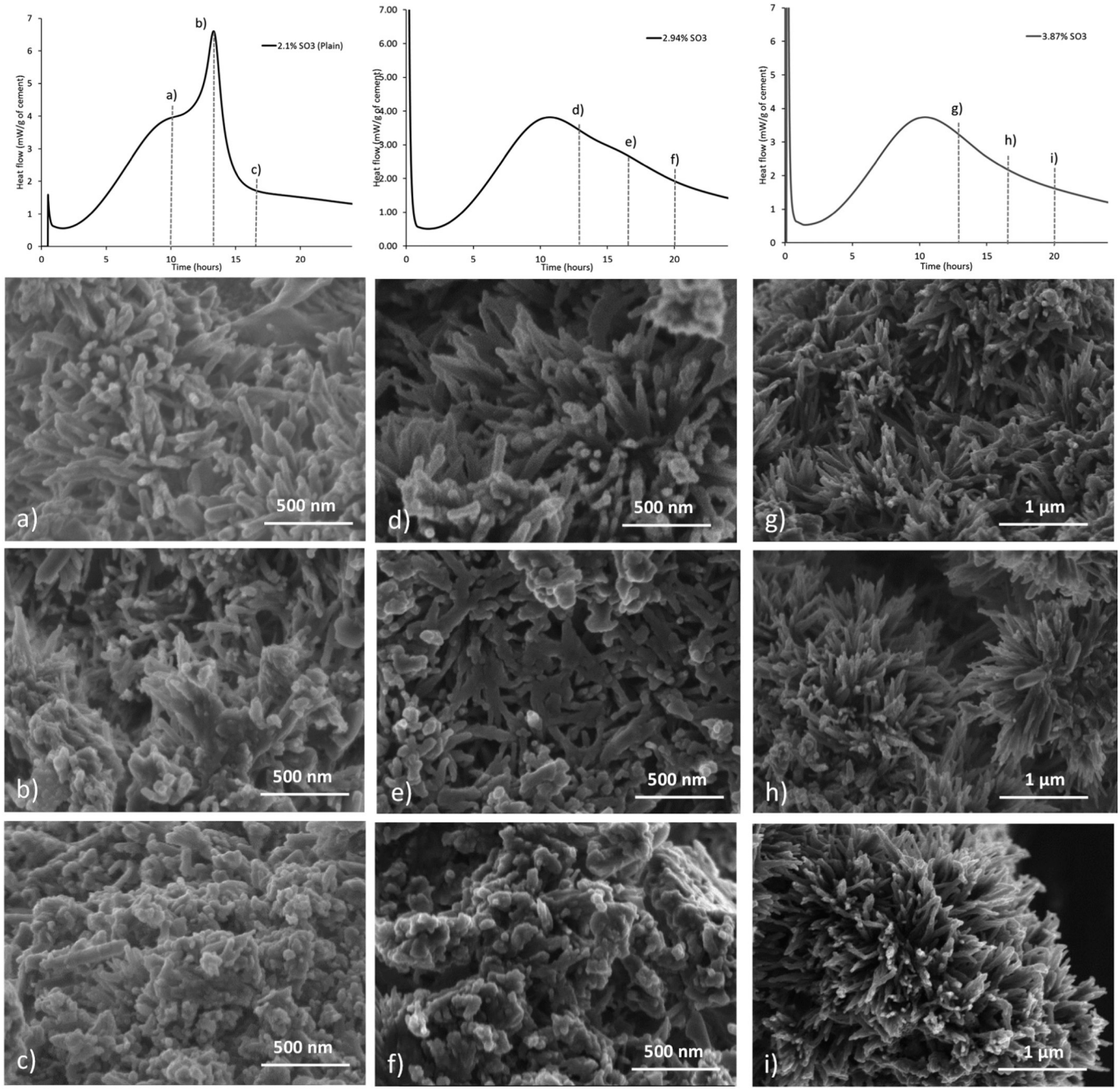

Fig. 7. SFEG-SEM micrographs showing the C-S-H morphology in the system with 2.1% total SO_3 (plain white cement) at a) 10 h b) 13 h c) 16 h of hydration; for the system with 2.94% total SO_3 at d) 13 h, e) 16 h, f) 20 h of hydration; and for the system with 3.87% total SO_3 at g) 13 h h) 16 h i) 20 h of hydration. A divergent C-S-H morphology is observed before the sulfate depletion. After the sulfate depletion, agglomerated C-S-H are formed. The calorimetry data on the upper side show the time at which each micrograph was taken, for each mix.

hydration for the white cement paste prepared with 4% extra gypsum. Since the gypsum is not yet depleted after 20 h of hydration in the system with 4% gypsum, it was decided to make the SFEG-SEM images at the same time as for the 2% gypsum system for comparison purposes. The micrographs show that the morphology of C-S-H remains as diverging needles up to 20 h of hydration in the system with 4% extra gypsum.

3.5. ^1H NMR relaxometry

3.5.1. NMR signal fractions

Fig. 8 shows the ^1H NMR results over the first 3 days of hydration for the plain white cement paste and for the pastes with 2% and 4% extra gypsum. Following Muller et al. [15,16], four water populations can be distinguished and quantified: water in crystalline phases: portlandite and ettringite (called "solid" water, Fig. 8a), water in C-S-H interlayer spaces (Fig. 8b), water in C-S-H gel pores (Fig. 8c) and water in capillary pores (Fig. 8d). Combining the CPMG and the Quad-Echo pulse sequences, all the water in hydrating cement pastes can be measured and quantified as, for sealed pastes, $I_{solid} + I_{CSH} + I_{gel} + I_{cap} = 1$, I being NMR signal fractions. More details about the NMR measurement procedure and signal analysis can be found in [15,16].

Over the first 12 h of hydration, the solid water signal (Fig. 8a), the

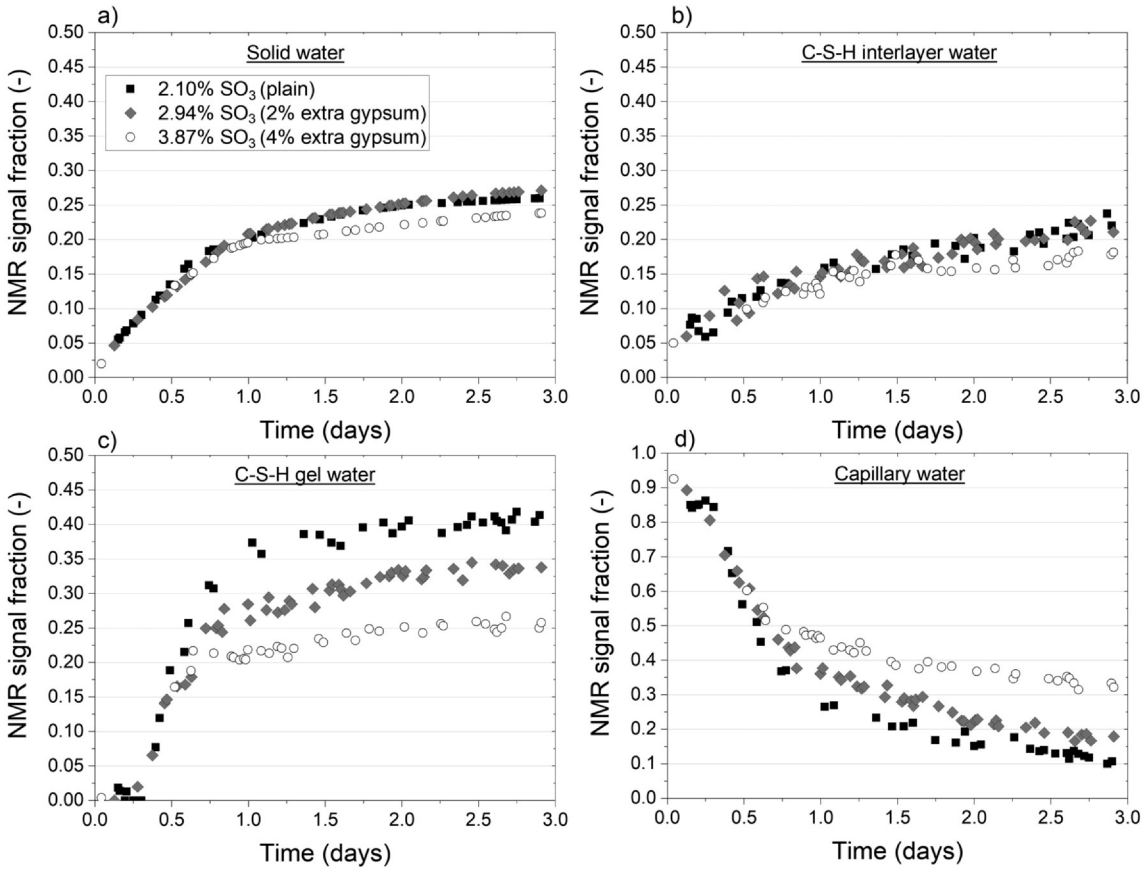

Fig. 8. Evolution of the different ^{1}H NMR signal fractions of different water populations for the plain white cement paste and when 2% and 4% of extra gypsum was added to the cement. a) Evolution of the solid water signal associated with water in Portlandite and ettringite. b) Evolution of the signal from the water in C-S-H interlayer spaces. c) Evolution of the signal from the water in C-S-H gel pores. d) Evolution of the signal from the water in capillary pores.

signal from C-S-H interlayer water (Fig. 8b) and the signal from C-S-H gel water (Fig. 8c) are all increasing rapidly in the same manner. Cement reacts with the capillary water to form cement hydrates. At 12 h, which corresponds to the maximum of the calcium silicate peak (see Fig. 3), all water signals are similar in all the systems studied. The solid signal fraction and the C-S-H interlayer signal fraction are at around 10% each. The fraction of gel water is about 15% and the fraction of capillary water is about 65% of all the water in each of the cement pastes.

Beyond 12 h of hydration, the solid signal and the C-S-H interlayer signal continue to increase similarly across the different mixes. However, the C-S-H gel water plateaus at different levels depending on the gypsum content of the cement (Fig. 8c). Increasing the gypsum content significantly reduces the amount of gel water detected by NMR in the long term. At 3 days, 40% of all the mixing water is detected in the C-S-H gel pores for the plain white cement paste. When 2% extra gypsum is added to the cement, the fraction of gel water is reduced to 32%. When 4% extra gypsum is added to the cement, the fraction of gel water is further reduced to 25%. Since the solid water fraction and the C-S-H interlayer water fraction remain almost unchanged in all 3 mixes, the lack of gel water results in more capillary water (Fig. 8d).

3.5.2. T_2 relaxation times

Fig. 9 shows the evolution of T_2 relaxation times associated to the signals from C-S-H interlayer water, from C-S-H gel water and from capillary water for each mix shown in Fig. 8. In the present study, T_2 relaxation times are similar to the ones reported in [15–17]. Average T_2 times between 2.75 and 3.00 days of hydration are given in Table 1.

T_2 relaxation times of the C-S-H interlayer water are measured at around 80 µs for all samples. The slight increase observed at early ages

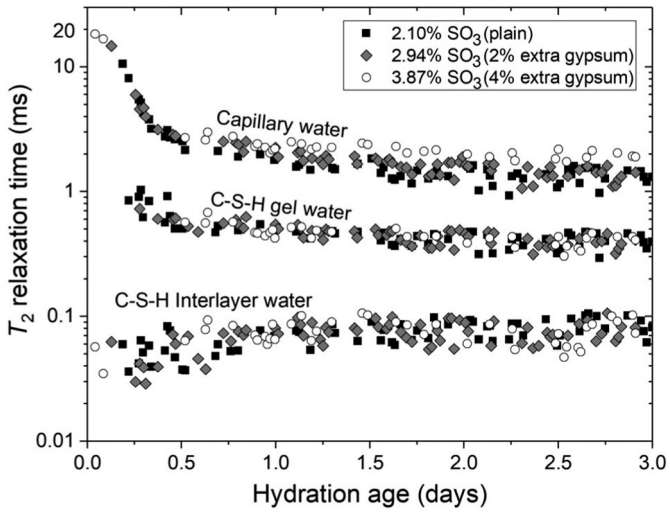

Fig. 9. Evolution of T_2 relaxation times of the C-S-H interlayer water, the C-S-H gel water and the capillary water for the plain white cement paste and the pastes with 2% and 4% additional gypsum over time. The error of measurement is given in Table 1.

is due to the difficulties to accurately determine short T_2 times when the signal is weak. T_2 relaxation times of the C-S-H gel water are also similar across the three system studied, from initially 600 µs to 400 µs after 2 days of hydration. This indicates that there is no fundamental changes in the nature of the C-S-H gel pores, even if the amount of gel water varies when changing the sulfate content of the cement (see

Table 1
Average T_2 relaxation times between 2.75 and 3.00 days of hydration for all water populations and all mixes. The error is given in the table.

	2.10% SO_3 (plain)	2.94% SO_3	3.87% SO_3
Interlayer water T_2 (± 10 μs)	81 μs	78 μs	81 μs
Gel water T_2 (± 40 μs)	397 μs	377 μs	407 μs
Capillary water T_2 (± 0.15 ms)	1.29 ms	1.28 ms	1.95 ms

Fig. 8c). T_2 relaxation times of the capillary pore water go down from initially 20 ms to 1–2 ms during the first 2 days of hydration. At 3 days of hydration, T_2 of the capillary water is 1.3 ms for the plain white cement paste and for the paste with 2% extra gypsum. When 4% of extra gypsum is added to the cement, this characteristic T_2 increases to around 2.0 ms.

Differences in T_2 imply a difference in pore size. T_2 relaxation times in ^{1}H NMR relaxometry can be related to the surface-to-volume ratio of the pore space thanks to the fast exchange model developed byBrownstein and Tarr [19] and Cohen and Mendelson [20]. Following the same methodology as in [15,16], the C-S-H gel pore size (i.e. where gel water is located) at 3 days of hydration is ~2.5 nm and the C-S-H interlayer pore size is ~0.8 nm at all times. 1.3 ms for T_2 of the capillary water corresponds to a pore size of around 10 nm. Similarly, a T_2 relaxation time of 2.0 ms corresponds to a pore size of 15 nm (case of the 4% gypsum mix). Please note that bigger capillary pores, not detected by NMR, exist due to chemical shrinkage and self-desiccation and that ^{1}H NMR only detects water filled pores.

3.6. SEM-EDX analysis

SEM-EDX analyses were made on the three pastes studied to evaluate the chemical composition of the C-S-H at 3 days of hydration. The results are shown graphically in Fig. 10 and the C-S-H molar ratios, obtained following the method of Rossen and Scrivener [21], are reported in Table 2. The main effect of increasing the sulfate content of the cement on the chemical composition of the C-S-H was an increase of the sulfate uptake in the C-S-H. The S/(Ca−S) ratio of the C-S-H was 0.010 in the plain cement paste system, which then increased to 0.024 for 2% added gypsum and further to 0.071 for 4% added gypsum. In parallel, neither the (Si + Al)/(Ca−S) nor Al/(Ca−S) was significantly affected by the addition of sulfate. No changes were observed to the Al content of the C-S-H by addition of extra gypsum for the reason that there is not enough Al available to significant change the Al content of the C-S-H (the white cement studied contains only 3.6% of C_3A).

3.7. Paste volume compositions at 3 days

Combining NMR and XRD data, the paste volume composition was calculated for each of the 3 mixes studied at 3 days of hydration. The volume of Portlandite, ettringite and remaining cement was calculated based on XRD phase quantification, assuming $\rho_{portlandite}$ = 2.24, $\rho_{ettringite}$ = 1.77 and ρ_{cement} = 3.15 g/cm^3. The volume of C-S-H layers was calculated based on the NMR C-S-H interlayer water signal, assuming an inverse mass fraction of water in C-S-H layers of 0.173 and ρ_{CSH} = 2.72, as in [15,16]. The volume of C-S-H gel water was taken from its respective NMR signal fraction, assuming a density of water in C-S-H gel pores of 1 g/cm^3. The sum of both interlayer volume and gel water volume defines the C-S-H bulk volume. The volume of capillary water was taken from its respective NMR signal fraction. The chemical shrinkage volume (voids) was calculated from the initial paste volume, i.e. water + cement volume upon mixing, minus the volume of all other phases. The resulting paste volume composition for the three samples studied is shown in Fig. 11. It can be observed that the volume of bulk C-S-H (and to a lesser extend Portlandite) goes down significantly with increasing the sulfate content of the cement. On the other hand, the volume of capillary pores and ettringite goes up with increasing the sulfate content.

3.8. SEM polished sections microscopy

The microstructure of hydrated cement pastes at 3 days of hydration was studied on polished sections for the plain white cement paste and the pastes with 2% and 4% extra gypsum. Fig. 12 shows representative SEM micrographs at low magnification (a, b and c) and at high magnification (d, e and f) for the three samples with the three different SO_3 contents. Black areas represent capillary pores in the microstructure.

Average values were calculated from a set of 400 images to evaluate the pore volume in each of the cement paste studied. The results are shown in Table 3. The evaluated porosity based on BSE-SEM images was 9% for the plain white cement paste, 12% for the paste with 2% added gypsum and 20% for the paste with 4% added gypsum. These values are in line with the ^{1}H NMR results (Fig. 8d) where more capillary water was detected in the system with 2% extra gypsum and even more in the system with 4% extra gypsum.

4. Discussion & conclusions

In this paper the hydration of plain white cement and white cement with 2% and 4% additional gypsum was studied by a multi-technique approach. This allowed for the first time correlating the reaction kinetics measured by calorimetry with the phase assemblage, composition and morphology of hydrates measured by XRD, NMR and SEM.

4.1. Depletion of gypsum and change in C-S-H gel water content and in C-S-H morphology

One of the main findings of this study is that there was a clear reduction of C-S-H gel water by the addition of extra calcium sulfate. Fig. 13a shows the development of the gel water content as measured by ^{1}H NMR compared to the heat released measured by calorimetry, for the three pastes studied. It highlights that the change in gel water content occurs at the same time as the gypsum depletion, which can be observed by calorimetry due to the renewal of the aluminate reaction.

SFEG-SEM micrographs presented in Fig. 7 revealed that the change in gel pore content was correlated with a change in C-S-H morphology, from needles-like before to agglomerated morphology after the sulfate depletion. Fig. 13b summarizes schematically using SEM micrographs the change in C-S-H morphology as a function of hydration time for all studied mixes. During the first 12 h of hydration, divergent C-S-H needles are observed in all three mixes and the same amount of gel water is detected by ^{1}H NMR. The depletion of the gypsum occurs at 12 h for the plain white cement paste (seen by calorimetry), time at which the C-S-H morphology changes from divergent needles to agglomerated C-S-H, along with the formation of more gel pores (detected by ^{1}H NMR). The depletion of the gypsum occurs at 16 h for the 2% gypsum paste, time at which the C-S-H morphology changes from divergent needles to agglomerated C-S-H, along with the formation of more gel pores (compared to the 4% gypsum mix). For the 4% gypsum mix, the divergent C-S-H needle morphology persists beyond 20 h and the amount of gel water is the lowest of all mixes studied.

The exact reason for the change in C-S-H morphology and the change in C-S-H gel pore content upon calcium sulfate depletion requires further investigations. Previous studies have shown that the sulfate depletion leads to drastic changes in the pore solution chemistry [22,23]: the sulfate concentration in the pore solution drops by about 20–60×, the aluminium concentration increases up to 100×, the calcium concentration is reduced by minimum 2× and an increase of pH is observed. Understanding the impact of each of these changes, or combination thereof, on the C-S-H characteristics requires further research.

Another interesting feature of the data is that the content of C-S-H interlayer water remains almost unchanged across the different mixes.

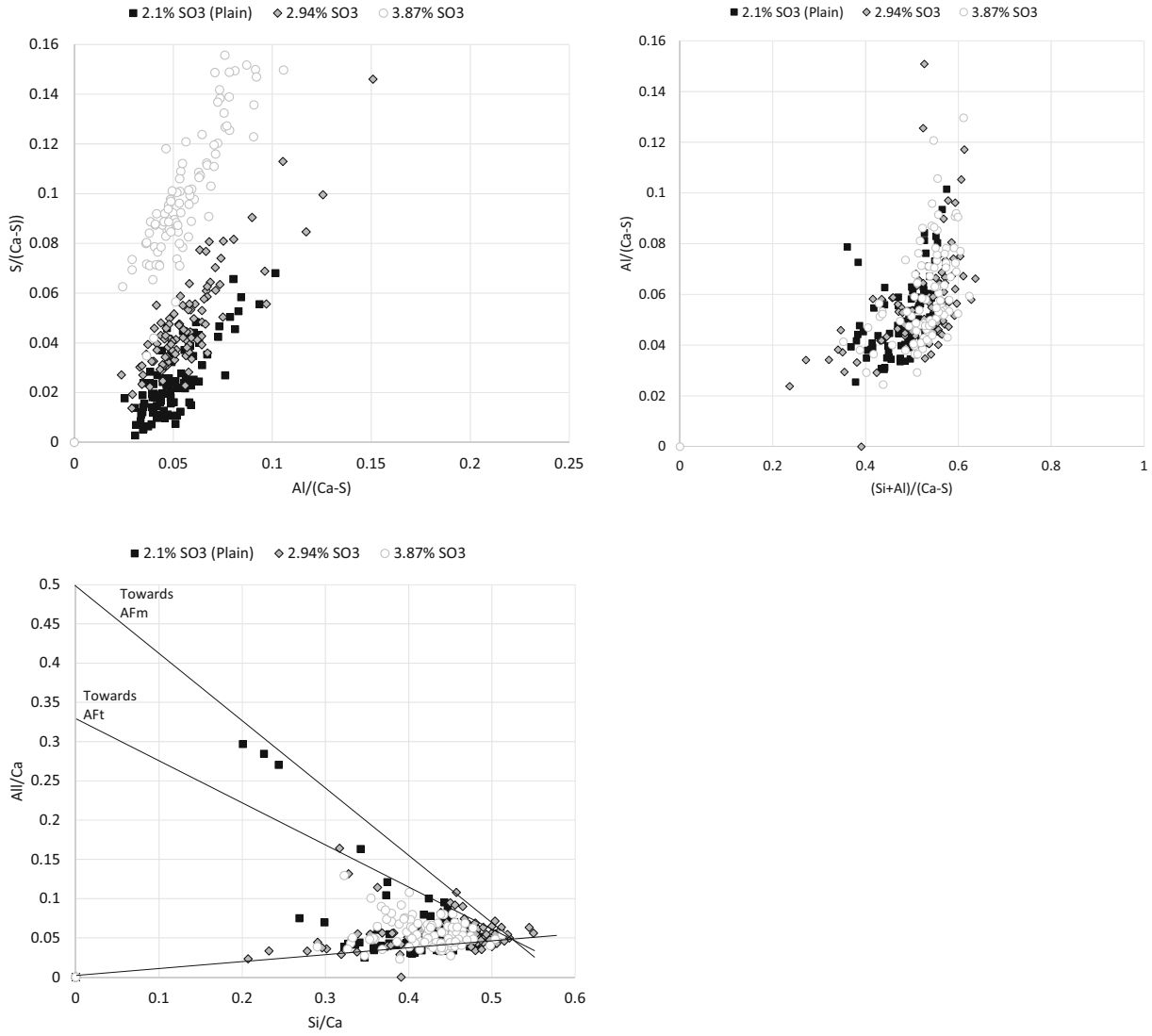

Fig. 10. Chemical composition of C-S-H at 3 days of hydration from SEM-EDX measurements. The data are presented as a function of cement sulfate content.

Table 2
Chemical composition of the C-S-H as measured by SEM-EDX and quantified by the method developed by Rossen and Scrivener (2017).

	Representative measurement error	2.10% SO_3 (plain)	2.94% SO_3	3.87% SO_3
S/(Ca-S)	± 0.010	0.010	0.024	0.071
(Si + Al)/(Ca-S)	± 0.05	0.60	0.62	0.61
Al/(Ca-S)	± 0.010	0.029	0.034	0.024
Si/Ca	± 0.05	0.48	0.53	0.49

This suggests that the creation of the elementary blocks of the C-S-H, i.e. the C-S-H layered structures, is not affected by the type of C-S-H morphology and changes in gel pore content. This has a great implication for the way gel pores are viewed and created.

Several concepts of gel pores have already been proposed. Feldman and Sereda in 1970 [24] depicted the gel pores as irregularities (or defects) into the C-S-H layer stacking. Jennings in 2008 [25] proposed the CM-II model where small stacks of C-S-H layers were viewed as globules that agglomerate, forming small gel pores (SGP) and large gel pores (LGP) between particle flocs. Recent NMR studies [15–17] concluded that gel pores must be strictly located inside C-S-H needles seen in SEM micrographs, and that the spaces between the C-S-H needles are the smallest capillary pores (called interhydrates).

C-S-H needles seen in SFEG-SEM micrographs in Fig. 7 are thick enough to contain ~7–10 Ca-Si-O backbone layers and ~2–3 gel pores across. The exact way gel pores are part of the needles is still unclear. Muller et al. [15,16] proposed a diagram similar to the Feldman and Sereda model [24] with disordered layers encompassing gel pores. The present study showed that the change of C-S-H morphology from divergent needles to agglomerated C-S-H was correlated with the formation of more gel pores. This closely matches the concept of the CM-II model from Jennings [25] where more gel pores can arise from agglomeration of globules. This suggests that the gel pores may not be fully restricted to the interior of the needles. Despite the changes occurring to the C-S-H morphology and to the C-S-H gel pore content, the gel pore size, as measured from ^{1}H NMR relaxometry (characteristic T_2), did not significant change.

4.2. C-S-H growth model

Many studies have been published with the aim to model cement hydration. Bishnoi et al. [26] developed the μic model which mimics the hydration of millions of cement particles in a given paste volume and the creation of hydration products around them. The slowdown of the reactions came from the impingement of the hydrates, but that

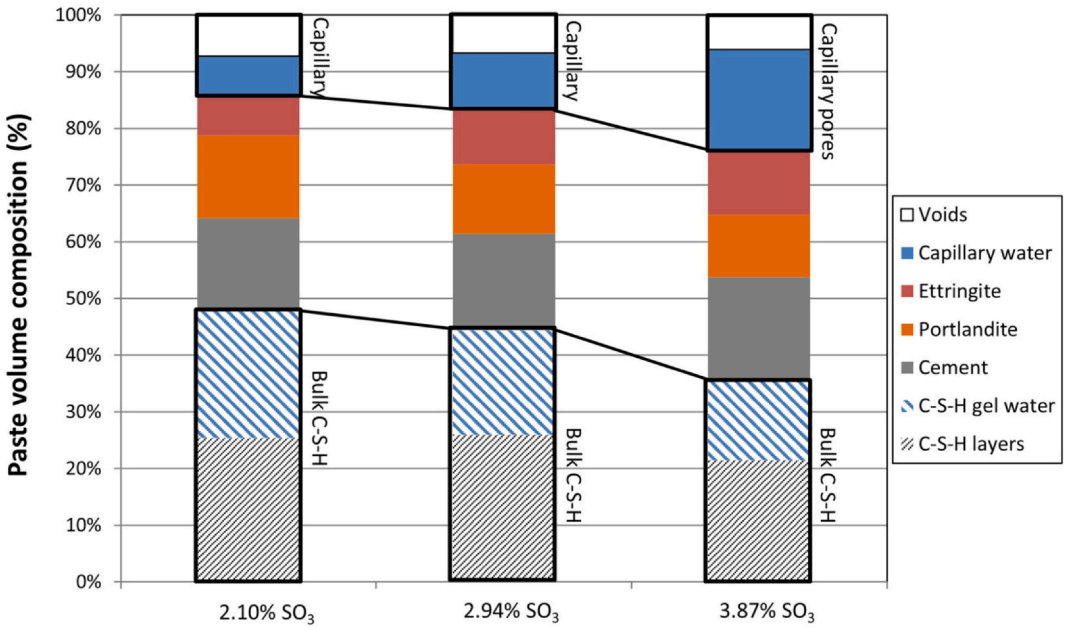

Fig. 11. Paste volume composition of the three cement pastes studied calculated based on XRD and NMR results.

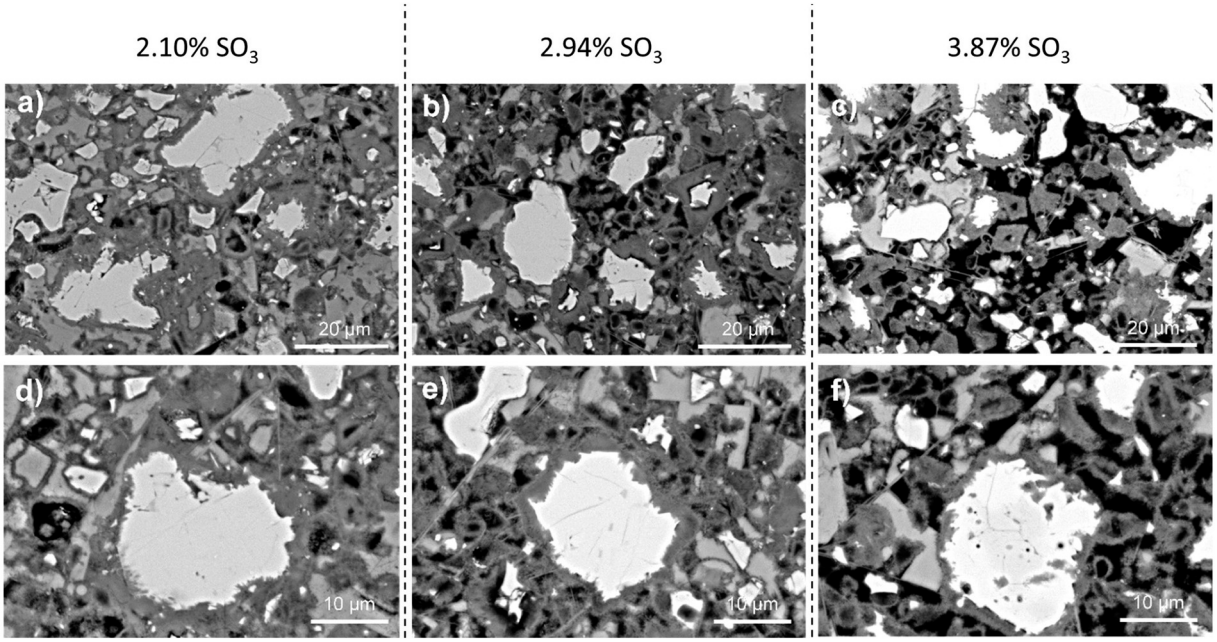

Fig. 12. SEM-BSE polished section microscopy at 3 days of hydration of a) and d) the plain white cement paste with 2.10% SO_3; b) and e) the white cement paste with 2.94% SO_3; c) and f) the white cement paste with 3.87% SO_3.

Table 3
Average porosity (in %) evaluated statistically from 400 backscattered SEM images for the plain white cement paste and the paste with 2% and 4% extra gypsum at 3 days of hydration.

System	2.10% SO_3 (plain)	2.94% SO_3	3.87% SO_3
SEM porosity (%)	9 ± 1.6	12 ± 1.4	20 ± 2

hypothesis was contradicted by the effect of varying water to cement ratio (Scrivener et al. [27]). More recently, Ouzia and Scrivener [28] built the "needle model" based on the nucleation and growth rates of C-S-H needles measured by Bazzoni [29]. In this model, the slowdown of the reactions coincided with the time at which most of the grain surfaces were covered with needles while the needles maintained their fast growth regime. Later on, the C-S-H needles enter into a slow growth regime.

So far, models relied on a non-evolving CSH morphology and density. CSH has mostly been modelled as layers of uniform thickness, or more recently as needles, but the evolution of the morphology over time was never considered. Furthermore, even though some models integrate the possibility to have varying CSH density, its coupling with sulfate addition (the increase of gel porosity upon gypsum depletion) is not considered. We suggest that future models consider these effects.

4.3. Capillary pore volume versus compressive strength

Fig. 14 compares the porosity calculated from ^{1}H NMR results with

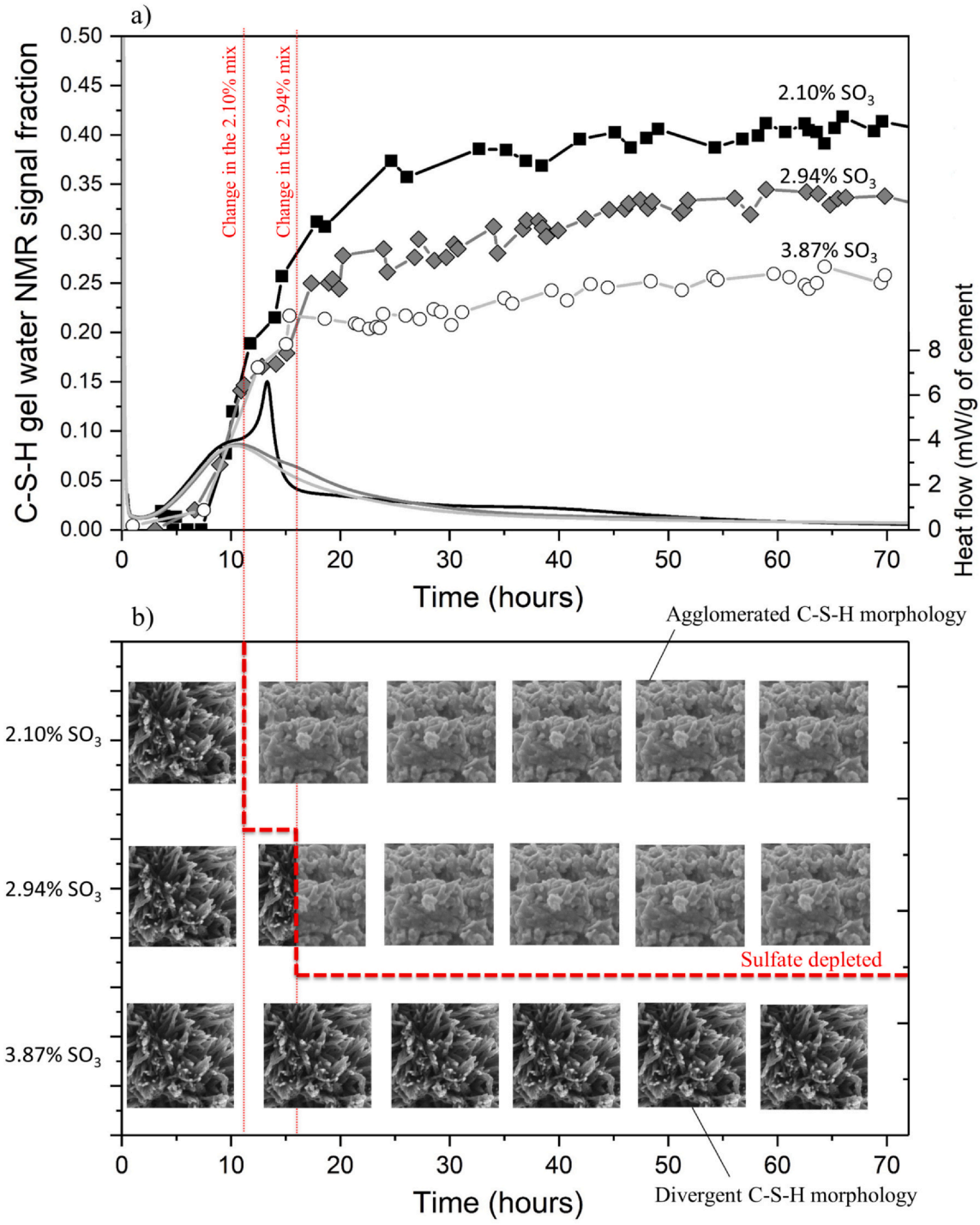

Fig. 13. a) Development of the gel pore content as measured by ^{1}H NMR for the white cement paste and the pastes with 2% and 4% extra gypsum. It shows the relationship between the formation of more gel pores and the depletion of the gypsum seen on the calorimetry results. The red lines indicate the gypsum depletion for the different mixes. b) Snapshots from SFEG-SEM micrographs representing the C-S-H morphology before and after the sulfate depletion. (For interpretation of the references to colour in this figure legend, the reader is referred to the web version of this article.)

the porosity calculated from SEM-BSE image analysis. Both results follow the same trend: the measured capillary porosity increases with increasing the sulfate content of the cement. The porosity measured by SEM is however systematically lower than the porosity measured by NMR. This was already observed by Muller et al. [17] and was attributed to the lower resolution of the microscopy technique which does not allow to measure the finest extend of the capillary porosity.

When comparing the compressive strength measured on standard mortars to the content of capillary porosity, it can be observed that the strength results do not correlate with the monotonic increase of the capillary pore volume when increasing the sulfate content. This indicates that not only the total pore volume is responsible for the strength performance of the binder but also, to some extent, the phase assemblage and the distribution of hydrates. The formation of more ettringite seems to be primarily responsible for the higher strength observed for the cement containing 2% extra gypsum (2.94% total SO_3), despite a slightly lower C-S-H volume and a slightly higher capillary porosity. For higher sulfate contents, the further formation of

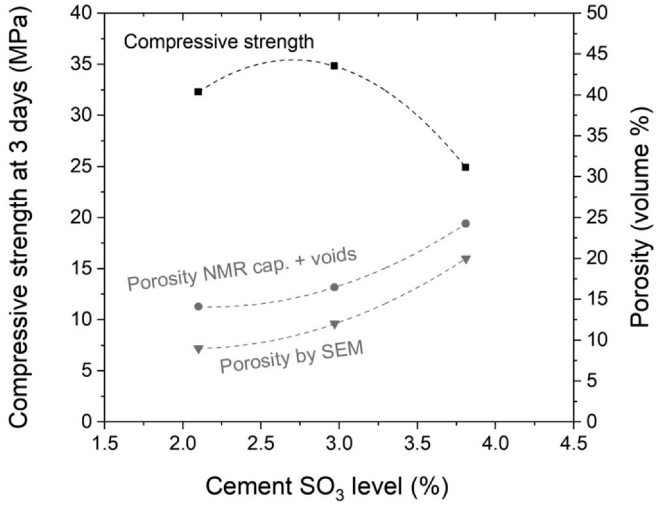

Fig. 14. Capillary porosity measured from ^{1}H NMR and from SEM-BSE image analysis as a function of the cement sulfate content, compared to the measured compressive strength on standard mortars. Doted lines are guide to the eye.

ettringite is not enough to compensate for the strong detrimental effect of extra sulfate on the C-S-H bulk volume. Similar conclusions were found by Zajac et al. [30].

Author statement

Elise M.J. Bérodier: Conceptualization, Methodology, Formal analysis, Writing - Original Draft, Investigation, Visualization, Writing - Review & Editing; Arnaud C.A. Muller: Conceptualization, Methodology, Formal analysis, Writing - Original Draft, Investigation, Visualization, Writing - Review & Editing, Project administration; Karen L. Scrivener: Conceptualization, Methodology, Formal analysis, Writing - Original Draft, Visualization, Writing - Review & Editing, Supervision, Funding acquisition.

Declaration of competing interest

The authors declare that they have no known competing financial interests or personal relationships that could have appeared to influence the work reported in this paper.

References

[1] F.A. Wilder, Gypsum: its occurrence, origin, technology and uses (pp.473-538), Iowa Geol. Surv. Annu. Rep. 28 (1919) 473–538, https://doi.org/10.17077/2160-5270.1207.
[2] P.S. Roller, The setting of Portland cement: chemical reactions and the role of calcium sulfate, Ind. Eng. Chem. 26 (1934) 669–677, https://doi.org/10.1021/ie50294a018.
[3] M. Collepardi, G. Baldini, M. Pauri, M. Corradi, Retardation of tricalcium aluminate hydration by calcium sulfate, J. Am. Ceram. Soc. 62 (1979) 33–35, https://doi.org/10.1111/j.1151-2916.1979.tb18800.x.
[4] J. Pommersheim, J. Chang, Kinetics of hydration of tricalcium aluminate in the presence of gypsum, Cem. Concr. Res. 18 (1988) 911–922, https://doi.org/10.1016/0008-8846(88)90027-0.
[5] R.F. Feldman, V.S. Ramachandran, Character of hydration of 3CaO.Al2O3, J. Am. Ceram. Soc. 49 (1966) 268–273, https://doi.org/10.1111/j.1151-2916.1966.tb13255.x.
[6] H. Minard, S. Garrault, L. Regnaud, A. Nonat, Mechanisms and parameters controlling the tricalcium aluminate reactivity in the presence of gypsum, Cem. Concr. Res. 37 (2007) 1418–1426, https://doi.org/10.1016/j.cemconres.2007.06.001.
[7] A. Quennoz, K.L. Scrivener, Hydration of C 3A-gypsum systems, Cem. Concr. Res. 42 (2012) 1032–1041, https://doi.org/10.1016/j.cemconres.2012.04.005.
[8] L. Nachbaur, P.C. Nkinamubanzi, A. Nonat, J.C. Mutin, Electrokinetic properties which control the coagulation of silicate cement suspensions during early age hydration, J. Colloid Interface Sci. 202 (1998) 261–268, https://doi.org/10.1006/jcis.1998.5445.
[9] A. Bentur, Effect of gypsum on the hydration and strength of C3S pastes, J. Am. Ceram. Soc. 59 (1976) 210–213, https://doi.org/10.1111/j.1151-2916.1976.tb10935.x.
[10] C. Labbez, M. Medala, P. Isabelle, A. Nonat, Adsorption of sulfate ions on negatively charged surfaces, 7th Liq. Matter Conf., Lund,. G-6, 2008.
[11] R. Barbarulo, H. Peycelon, S. Prene, Experimental study and modelling of sulfate sorption on calcium silicate hydrates, Ann. Chim. Sci. Des Matériaux. 28 (2003) S5–S10.
[12] A. Quennoz, K.L. Scrivener, Interactions between alite and C3A-gypsum hydrations in model cements, Cem. Concr. Res. 44 (2013) 46–54, https://doi.org/10.1016/j.cemconres.2012.10.018.
[13] S. Gunay, S. Garrault, A. Nonat, P. Termkhajornkit, Influence of calcium sulphate on hydration and mechanical strength of tricalcium silicate, 13th Int. Congr. Chem. Cem. Madrid, Spain, 2011.
[14] B. Mota, T. Matschei, K. Scrivener, The influence of sodium salts and gypsum on alite hydration, Cem. Concr. Res. 75 (2015) 53–65, https://doi.org/10.1016/j.cemconres.2015.04.015.
[15] A.C.A. Muller, K.L. Scrivener, A.M. Gajewicz, P.J. McDonald, Use of bench-top NMR to measure the density, composition and desorption isotherm of C-S-H in cement paste, Microporous Mesoporous Mater. 178 (2013) 99–103, https://doi.org/10.1016/j.micromeso.2013.01.032.
[16] A.C.A. Muller, K.L. Scrivener, A.M. Gajewicz, P.J. McDonald, Densification of C-S-H measured by 1H NMR relaxometry, J. Phys. Chem. C 117 (2013) 403–412, https://doi.org/10.1021/jp3102964.
[17] A.C.A. Muller, Characterization of Porosity & C-S-H in Cement Pastes by 1H NMR, Ecole Polytechnique Fédérale de Lausanne (EPFL), (2014).
[18] E. Gallucci, P. Mathur, K. Scrivener, Microstructural development of early age hydration shells around cement grains, Cem. Concr. Res. 40 (2010) 4–13, https://doi.org/10.1016/j.cemconres.2009.09.015.
[19] K.R. Brownstein, C.E. Tarr, Importance of classical diffusion in NMR studies of water in biological cells, Phys. Rev. A 19 (1979) 2446–2453, https://doi.org/10.1103/PhysRevA.19.2446.
[20] M.H. Cohen, K.S. Mendelson, Nuclear magnetic relaxation and the internal geometry of sedimentary rocks, J. Appl. Phys. 53 (1982) 1127–1135, https://doi.org/10.1063/1.330526.
[21] J.E. Rossen, K.L. Scrivener, Optimization of SEM-EDS to determine the C–A–S–H composition in matured cement paste samples, Mater. Charact. 123 (2017) 294–306, https://doi.org/10.1016/j.matchar.2016.11.041.
[22] B. Lothenbach, F. Winnefeld, Thermodynamic modelling of the hydration of Portland cement, Cem. Concr. Res. 36 (2006) 209–226, https://doi.org/10.1016/j.cemconres.2005.03.001.
[23] S. Adu-Amankwah, M. Zajac, C. Stabler, B. Lothenbach, L. Black, Influence of limestone on the hydration of ternary slag cements, Cem. Concr. Res. 100 (2017) 96–109, https://doi.org/10.1016/j.cemconres.2017.05.013.
[24] R.F.S. Feldman P J, A new model for hydrated Portland cement and its practical implications, Eng. J 53 (1970) 53–59.
[25] H.M. Jennings, Refinements to colloid model of C-S-H in cement: CM-II, Cem. Concr. Res. 38 (2008) 275–289, https://doi.org/10.1016/j.cemconres.2007.10.006.
[26] S. Bishnoi, K.L. Scrivener, μic: a new platform for modelling the hydration of cements, Cem. Concr. Res. 39 (2009) 266–274, https://doi.org/10.1016/j.cemconres.2008.12.002.
[27] K. Scrivener, A. Ouzia, P. Juilland, A. Kunhi Mohamed, Advances in understanding cement hydration mechanisms, Cem. Concr. Res. 124 (2019) 105823, , https://doi.org/10.1016/j.cemconres.2019.105823.
[28] A. Ouzia, K. Scrivener, The needle model: a new model for the main hydration peak of alite, Cem. Concr. Res. 115 (2019) 339–360, https://doi.org/10.1016/j.cemconres.2018.08.005.
[29] A. Bazzoni, Study of Early Hydration Mechanisms of Cement by Means of Electron Microscopy, EPFL, Lausanne, Switzerland, 2014.
[30] M. Zajac, J. Skocek, A. Müller, M. Ben Haha, Effect of sulfate content on the porosity distribution and resulting performance of composite cements, Constr. Build. Mater. 186 (2018) 912–919, https://doi.org/10.1016/j.conbuildmat.2018.07.247.